Modelling of ITER Improved H-mode Operation with the Integrated Core Pedestal SOL Model

G. W. Pacher 1), H. D. Pacher 2), G. Janeschitz 3), A. S. Kukushkin 4), A. Pankin 5), G. Pereverzev 6), I. Voitsekhovitch 7)

1) Hydro-Québec, Varennes, Québec, Canada
2) INRS-EMT, Varennes, Québec, Canada
3) FZK-PL-Fusion, Karlsruhe, Germany
4) ITER IT, Garching, Germany
5) SAIC, San Diego, USA
6) Max-Planck Institut für Plasmaphysik, Garching, Germany
7) Euratom/UKAEA Fusion Association, Abingdon, United Kingdom

e-mail contact of the main author: pacher.guenther@ireq.ca

Abstract. The Integrated Core-Pedestal-SOL model is extended to model improved H-modes by including a stabilization which depends on the sparseness of low-order rational surfaces. The parameters, adjusted for Asdex-UG, reproduce the improvement in confinement observed in JET. If additional neoclassical impurity accumulation can be reduced or eliminated, the model gives an improvement of ITER performance at reduced plasma current, thus extending the pulse length even for the non-optimized conditions investigated.

1. Introduction

The Integrated Core-Pedestal-SOL (ICPS) model first introduced in [1] has been continuously modified and improved [2, 3, 4], so that it now models core energy transport with the MMM95 transport coefficients, stabilized by a combination of ExB velocity flow shear and magnetic shear in order to obtain an edge pedestal. The stabilization parameters are calibrated against experimental results of JET and Asdex-UG [4]. For ITER modelling, the boundary conditions (separatrix parameters) for the core model are self-consistently determined by scaling relationships, obtained from a database of B2-Eirene runs for the ITER SOL and divertor [5, 6, and references therein]. The model also includes neoclassical accumulation of the carbon intrinsic impurity [7], with a separatrix density determined from B2-Eirene modelling [6].

2. Validation against Asdex-UG

In [4], it was noted that the pedestal electron temperatures then predicted by the model were systematically higher than the AUG experimental values, whereas the ion temperatures showed much better agreement. Following [8], ETG transport, which is not stabilized by flow shear, has been added to the electron channel. Also, the beam particle source previously used was too small by a factor of almost two, and this is now corrected. With these improvements, good agreement is now obtained for both electron and ion pedestal temperatures in AUG. Fig.1 shows the comparison between the presently obtained edge parameters with those obtained in [4]. (Note that, in [4], the edge parameters were plotted at a radius determined from a strong change in the slope of electron temperatures. With the ETG transport added, this criterion is no longer very sensitive, so in fig. 1, values at the 95% flux surface are plotted instead). In similar JET simulations (not shown) the corrected fuelling source results in a less

flat density profile than previously obtained. Overall, for both devices the agreement between model and experiment is significantly improved.

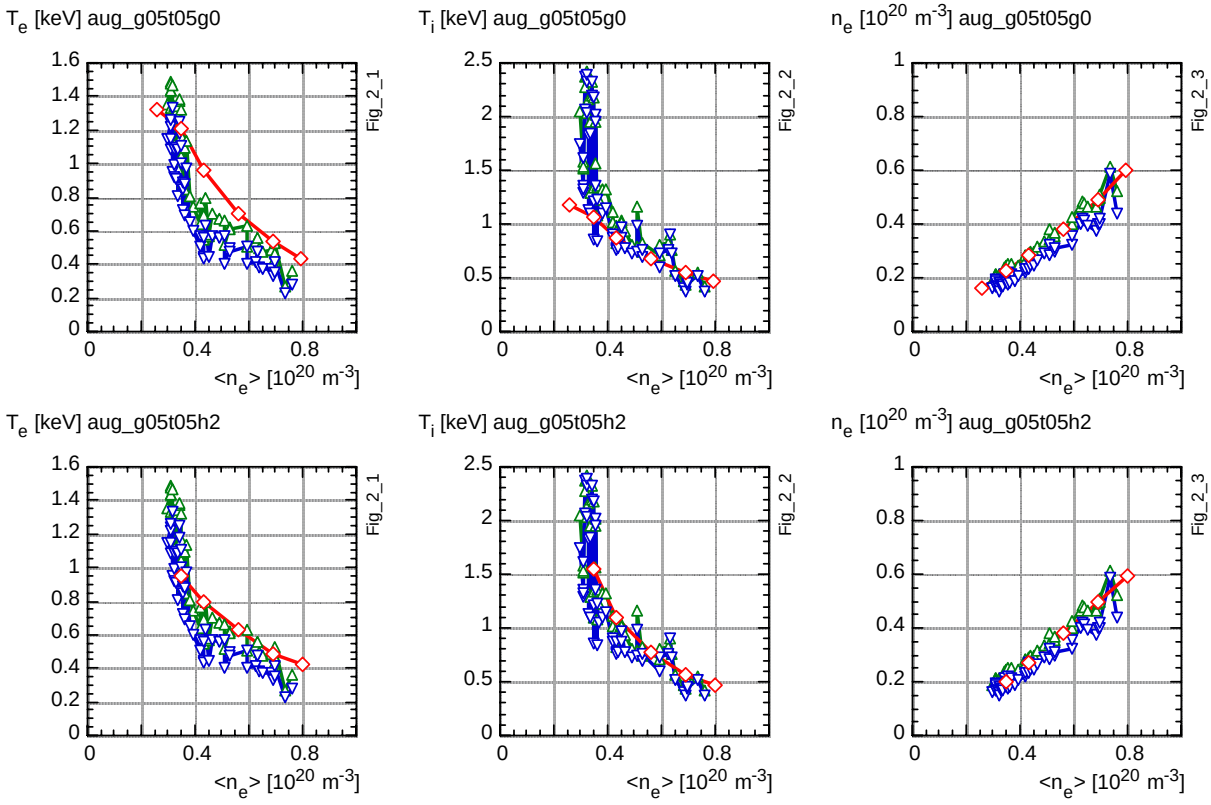

Fig. 1. Comparison of simulations (red lines and symbols) with experimental database for Asdex-UG for temperatures of electrons (left), ions (middle), and electron density (right). The values at the 95% flux surface are plotted. Top row shows the results without ETG and with the previously specified fuelling profile as in [4]. Bottom row shows the improved fit with ETG and with the corrected fuelling profile.

3. Improved H-modes

Improved H-modes, characterized by low magnetic shear with central q close to but somewhat larger than unity, have been achieved in AUG with off-axis current drive by neutral beams [9]. Such H-modes are considered promising candidates to obtain improved confinement in ITER.

To model this operation, we postulate, as suggested in [10], that turbulent transport is reduced in regions for which the low order rational q surfaces are sparse. Accordingly, we define a function that depends on the difference of the spatial distribution of low order rational surfaces for a reversed or flat q profile as compared with the normal profile (Fig.2). "Low-order rational" surfaces are defined as those for which the number of toroidal circuits to field line closure is not large (below about ten). The sparseness function is given by the number of rational surfaces within a characteristic width from the point under consideration, weighted by the inverse of the number of toroidal circuits times the distance from the point. The function is normalised to its integral over the radius. The characteristic width used is proportional to a mixing length $\sim\sqrt{\rho_{i,tor}\cdot R}$ [e.g.11]. (Similar results are obtained for a characteristic length $\sim\sqrt{\rho_{e,pol}\cdot a}$). The sparseness function is shown in Fig. 2; it is seen that it allows a reasonable discrimination between normal and reversed or flat q profiles for a value of 0.1 to 0.15 for the three machines investigated.

Fig. 2a). Function representing the density of rational surfaces (circular plasmas) for parameters of AUG (left), for q profiles shown at right.

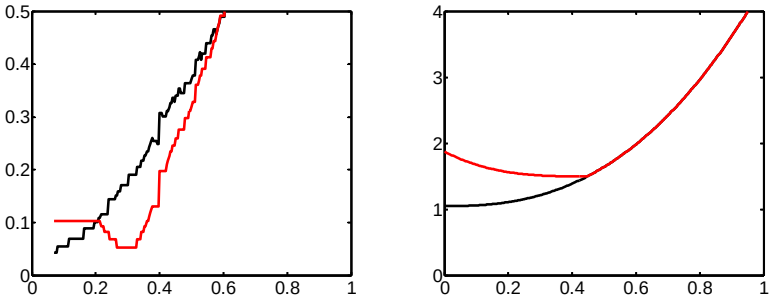

Fig. 2b). Function representing the density of rational surfaces (circular plasmas) for parameters of JET(left)), and ITER (right) for q profiles of Fig. 2a.

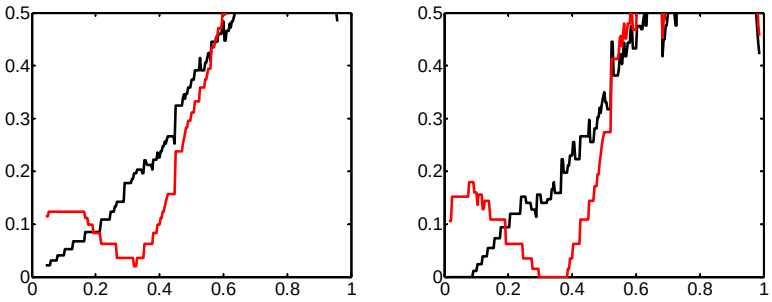

Fig. 2c). Function representing the density of rational surfaces (circular plasmas) for parameters of AUG (left), for less flat q profiles at right.

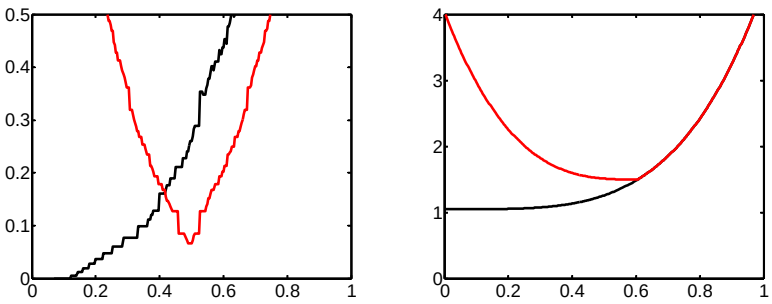

In the simulations, the effect of the sparseness of rational surfaces is implemented by reducing the transport by a predetermined factor when the function defined above drops below a threshold value of 0.1 (no confinement improvement is taken for q values close to unity because sawteeth act there). The strength of the stabilization is adjusted for AUG parameters approximating those of discharge #15524 as given in [9]. Fig. 3 shows the result, where profiles are plotted for normal q profile, flattened q profile without additional reduction, and reduction factors F of 1/5 and 1/10. For the same heating power profile (2.5 MW on axis, 2.5 MW at mid-radius), the H factor (H98y2) in AUG rises from 1.02 by 26% for F=1/5 and by 31% for F=1/10 with respect to the normal q profile (of this, the flattening of the q profile before application of the reduction factor alone accounts for 11%).

The same technique is applied for JET parameters with the same edge q as for the AUG discharge (fig.4). The heating profile is taken to be fairly broad and centred on axis. Current drive is applied in the simulations to produce flattened q profiles similar to those obtained in AUG. However, the current drive in these simulations is not accompanied by power deposition, so that this represents conditions where the current profile is established during rampup and frozen in thereafter (time-dependent simulations to model this more completely are planned). For these conditions, the H factor (H98y2) in JET rises from 0.64 to 1.05 (64% increase) for F=1/5 and to 1.13 for F=1/10 with respect to the normal q profile (for the flattened q profile alone it is 0.83). The improvement in H-factor for the case F=1/5 is comparable to the experimental result reported in [12].

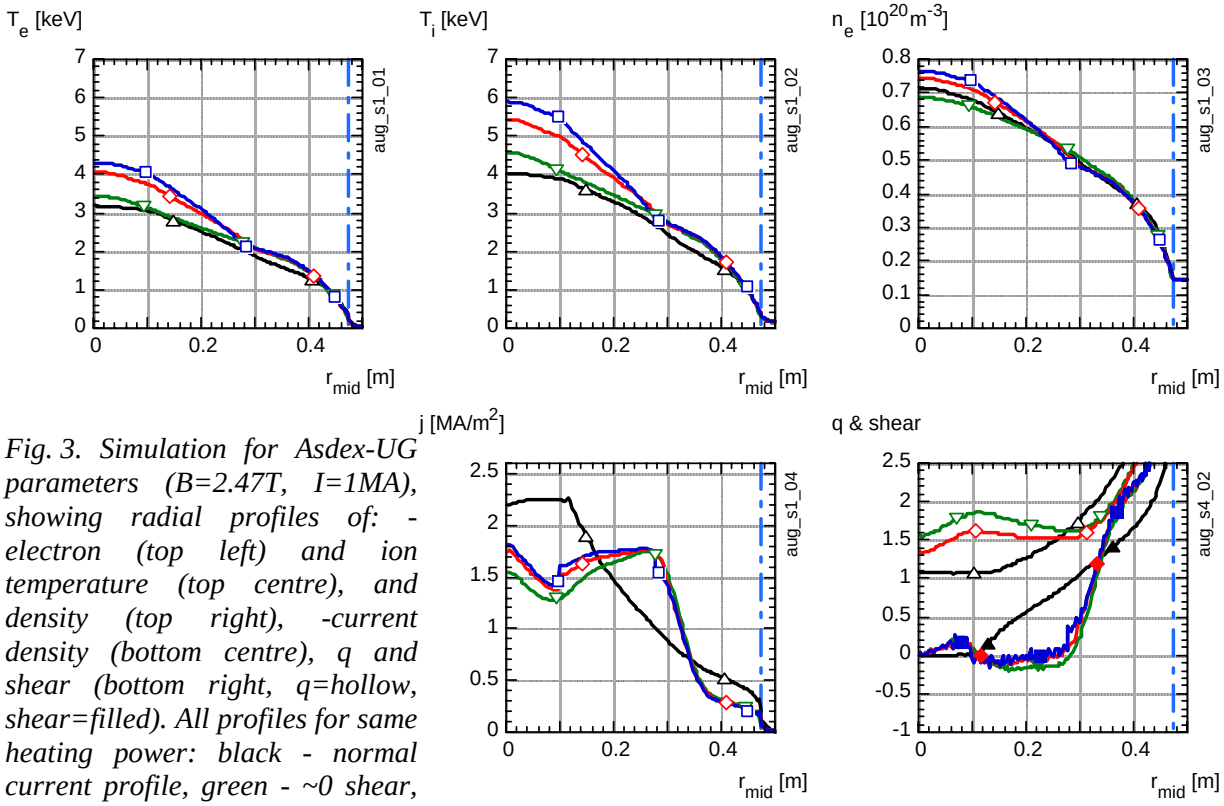

Fig. 3. Simulation for Asdex-UG parameters (B=2.47T, I=1MA), showing radial profiles of: - electron (top left) and ion temperature (top centre), and density (top right), -current density (bottom centre), q and shear (bottom right, q=hollow, shear=filled). All profiles for same heating power: black - normal current profile, green - ~0 shear, red - ~0 shear with transport reduction of 1/5, blue - ~0 shear with transport reduction 1/10.

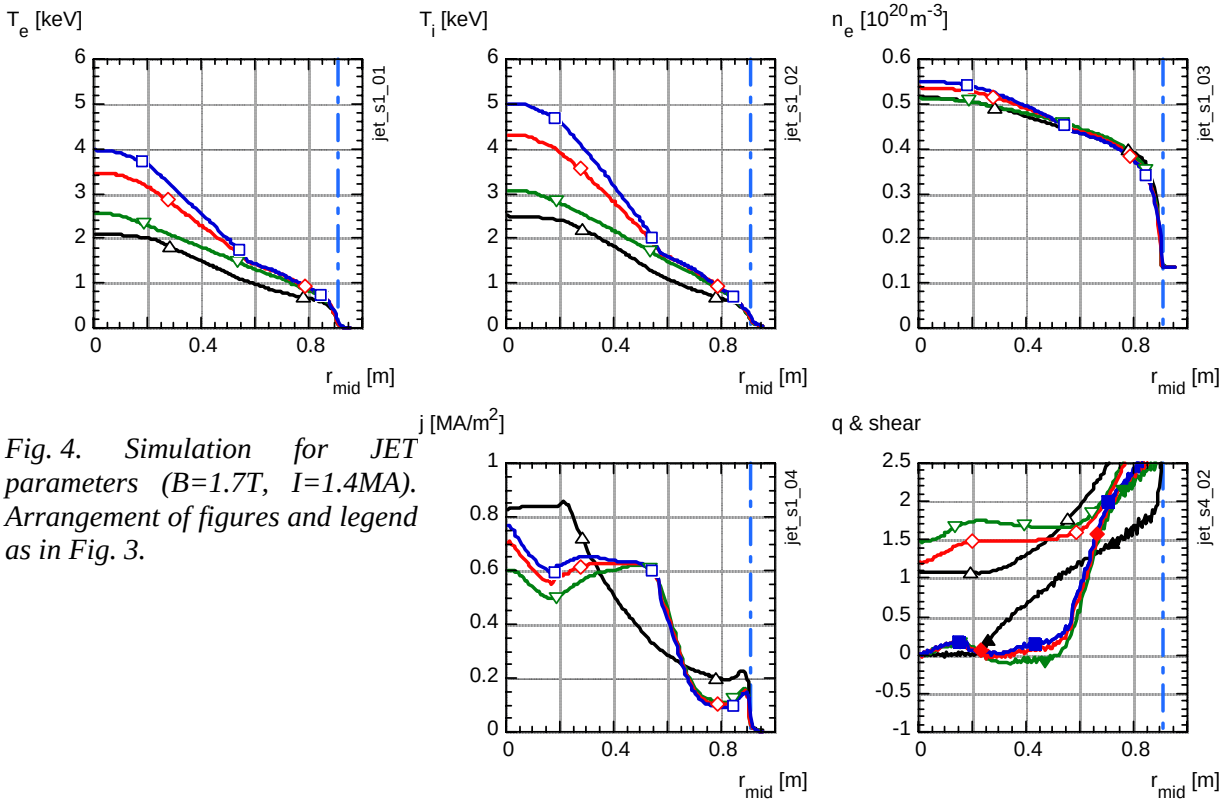

Fig. 4. Simulation for JET parameters (B=1.7T, I=1.4MA). Arrangement of figures and legend as in Fig. 3.

Thus, the characteristics of the improved H mode for both these devices are quite well simulated by this model. However, it should be pointed out that the ExB stabilisation applied to the edge to obtain the pedestal was not applied in the main part of the plasma and that the ExB stabilisation included in the MMM model was not yet activated; this remains to be done but is not expected to be very important for these conditions because the transport is already largely reduced by the effects discussed above.

In the course of this work, we have also briefly applied the model to conditions for which a hot ion mode would be obtained in JET [13]. In that preliminary investigation, the model (which contains MMM transport) included ExB stabilisation over the entire profile but did not take into account the stabilisation discussed above. Large ratios of ion to electron temperatures were not found even when equipartition was turned off for demonstration purposes. Further simulations should be undertaken to determine whether the ion transport included in the MMM model is too large under these conditions.

4. Application to ITER parameters

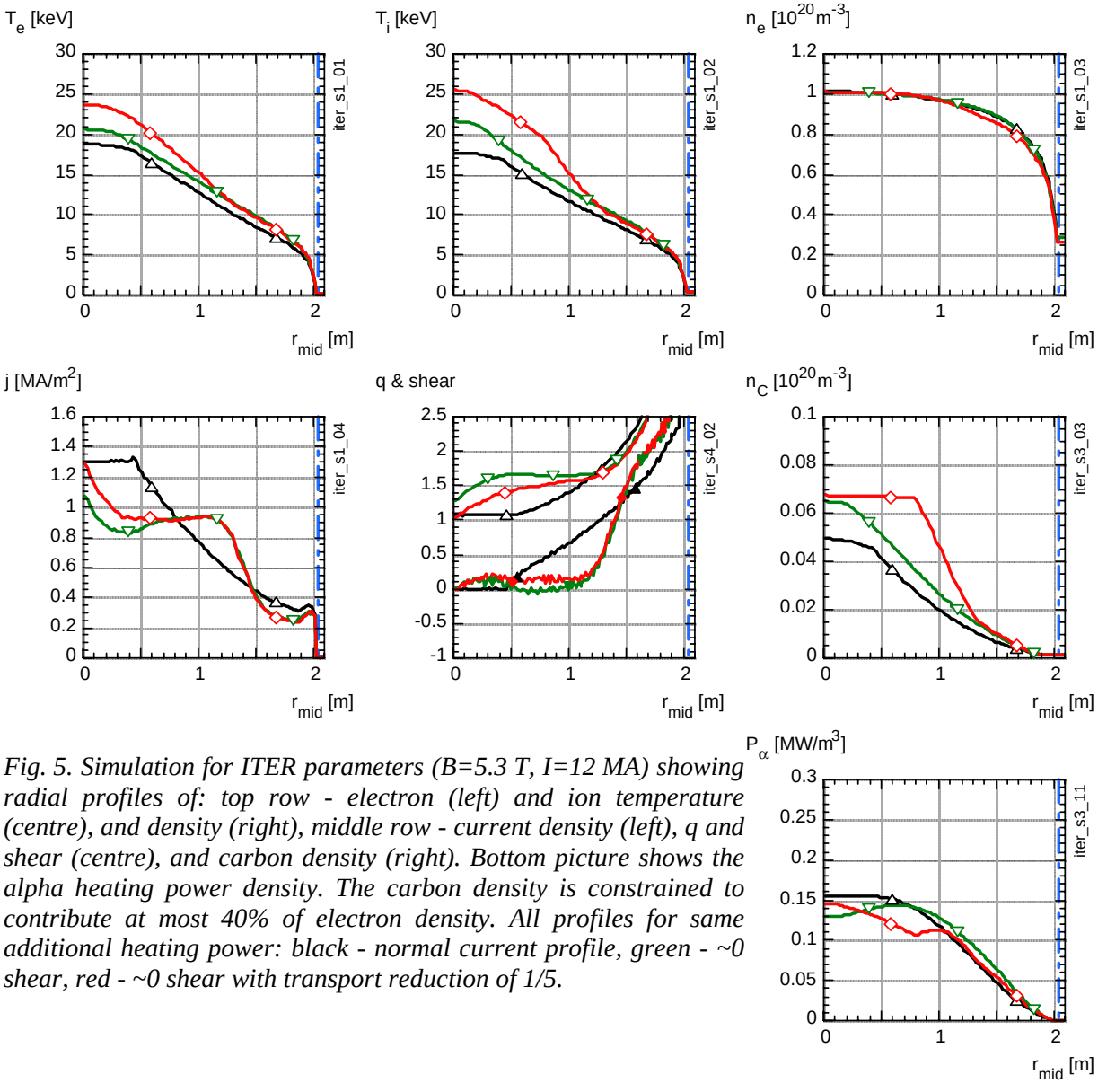

Fig. 5. Simulation for ITER parameters (B=5.3 T, I=12 MA) showing radial profiles of: top row - electron (left) and ion temperature (centre), and density (right), middle row - current density (left), q and shear (centre), and carbon density (right). Bottom picture shows the alpha heating power density. The carbon density is constrained to contribute at most 40% of electron density. All profiles for same additional heating power: black - normal current profile, green - ~0 shear, red - ~0 shear with transport reduction of 1/5.

For application to ITER, current drive is applied (again no heating power is associated with current drive, i.e. this also represents conditions where the q profile is established and frozen in during rampup) such that the resulting q profiles are similar to those obtained for AUG and JET. The total current is reduced to 12 MA, resulting in an edge q of ~4.5. The examples discussed have 50 MW of additional heating.

The resulting profiles are shown in Fig. 5 for an average density of ~90% of the Greenwald limit n_{GW}. When the stabilisation due to the sparseness of rational surfaces is applied, both electron and ion temperatures rise and the H factor increases by 20% (from H98y2 = 1.25 to 1.47), half of which is the direct result of the flattened q profile, and the other half comes from the transport reduction by a factor of 5 in the flat q region.

Despite the improved confinement demonstrated here, the fusion power does not increase with the transport reduction when the full ICPS model as described in [4] is used. This model includes carbon as an impurity, with the neoclassical equilibrium impurity profile determined according to the formulation of [7]:

$$n_C(r) = n_{C-sep}\ \exp\left\{\int_a^r \left(\frac{v_{an}+v_{coll}}{D_{an}+D_{coll}}\right)dr\right\}$$

$$D_{an} = 0.1(\chi_e + \chi_i),\ v_{an}\ \text{assumed zero}$$

$$D_{coll} = D_{Pfirsch-Schlüter} + D_{banana-plateau}$$

$$v_{coll} = -Z\left\{D_{Pfirsch-Schlüter}\left(\frac{1}{L_n} - \frac{1}{2L_T}\left(1-\frac{1}{Z}\right)\right) + D_{banana-plateau}\left(\frac{1}{L_n} + \frac{3}{2L_T}\left(1-\frac{1}{Z}\right)\right)\right\} + v_{Ware\ pinch}$$

L_n, L_T - gradient scale lengths for density and ion temperature

where the anomalous diffusion coefficient is taken to be $0.1\ (\chi_e+\chi_i)$. In integrated modelling, the central carbon density therefore increases as the anomalous diffusion coefficient is reduced. The resulting dilution even reduces the alpha heating power density somewhat (Fig. 5) despite the increase in central temperature. The corresponding total fusion power goes from 260 MW with the normal profile to 253 MW. It should be noted that only equilibrium impurity profiles are used in the simulation. A time-dependent calculation would therefore give higher fusion powers transiently which would relax as the impurity accumulates, with a transition time which remains to be determined.

Impurity accumulation may be less strong than that obtained above. On the one hand, instabilities such as the fishbones observed for flat q profiles may limit impurity accumulation without seriously affecting confinement [12]. On the other hand, active measures could be envisaged to reduce or eliminate impurity accumulation, such as central electron heating which was successfully applied to prevent impurity accumulation in AUG [9].

In order to demonstrate potential improvements if the increased impurity accumulation can be avoided, further simulations have been carried out. If the additional accumulation associated with stabilization via the sparseness function can be avoided, a fusion power of 325 MW is obtained at 0.9 n_{GW}, and of 440 MW at 1.1 n_{GW}. If passive or active mitigation is successful in maintaining the carbon profile similar to that obtained for the normal current profile case, the peak alpha heating power density increases (fig. 6). The corresponding total fusion power then rises from 260 MW to 436 MW (Q ~ 5 initially in this low-current case, rising to Q ~ 8.5 in the improved H-mode condition).

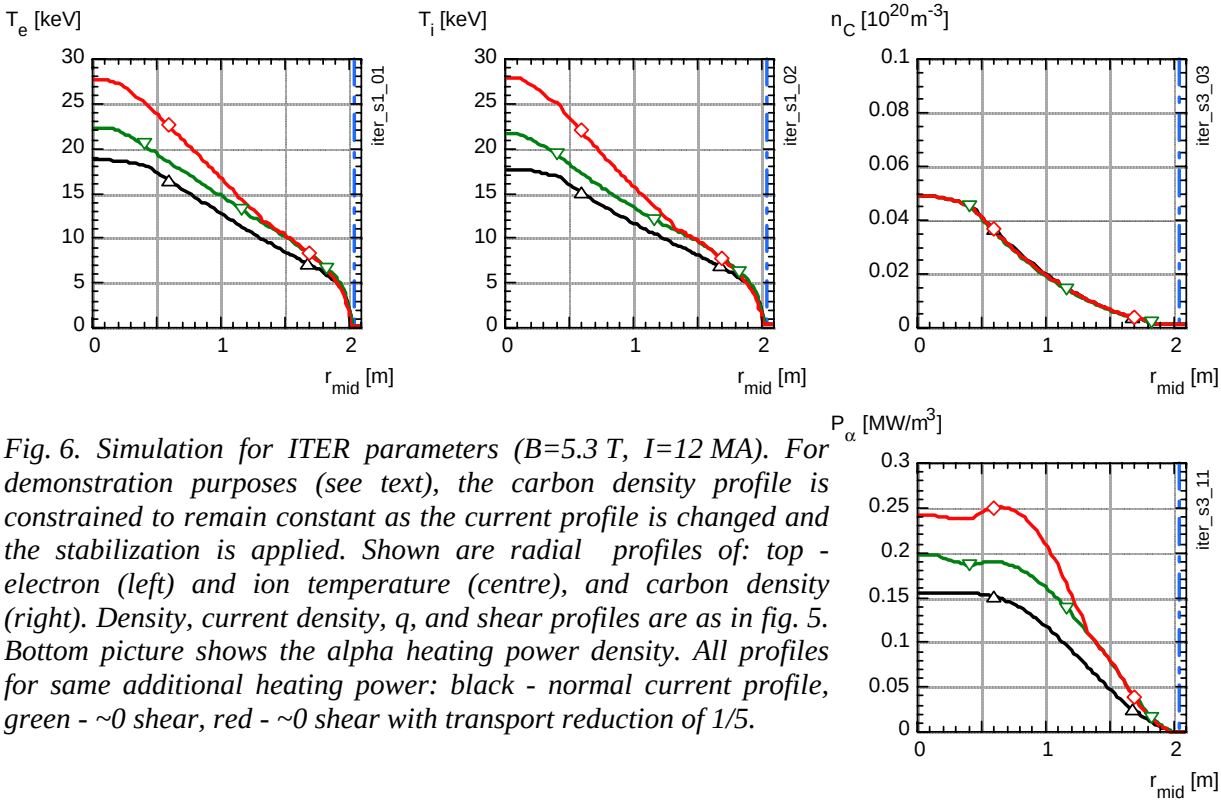

Fig. 6. Simulation for ITER parameters (B=5.3 T, I=12 MA). For demonstration purposes (see text), the carbon density profile is constrained to remain constant as the current profile is changed and the stabilization is applied. Shown are radial profiles of: top - electron (left) and ion temperature (centre), and carbon density (right). Density, current density, q, and shear profiles are as in fig. 5. Bottom picture shows the alpha heating power density. All profiles for same additional heating power: black - normal current profile, green - ~0 shear, red - ~0 shear with transport reduction of 1/5.

5. Conclusions

Improvements in the electron heat transport model and the description of the beam particle source have been implemented and lead to improved agreement between the simulations and the Asdex-UG database for H-mode pedestal parameters.

Modelling of improved H-modes has commenced. The approach, implemented in the integrated ICPS model, is based on stabilization related to the sparseness of rational surfaces which accompanies flat q profiles. The model parameters have been adjusted to simulate improved H-modes obtained in Asdex-UG. The same model applied to JET then gives reasonable agreement for the increase of the H-factor observed in improved H-modes.

The model has been applied to ITER, with the same flattened q profile as obtained in the Asdex-UG and JET simulations, representing ITER conditions where the flattened q profile is established during rampup and then frozen in for the resistive time scale. In ITER, improved confinement is obtained, but the fusion power decreases in equilibrium because of neoclassical accumulation of the intrinsic carbon impurity (if carbon is present in ITER) in the integrated model in which energy and particle confinement improve simultaneously. During the transition time toward equilibrium impurity accumulation, the fusion power would be appreciably higher than for the normal q profiles. If passive or active mitigation measures to reduce impurity accumulation are effective, a fusion power larger than 400 MW at Q values near 10 could be obtained in these as yet non-optimized conditions.

Further work will concentrate on detailed improvement and validation of the stabilization model, validation of the impurity accumulation and implementation of time-dependent impurity transport, and optimization of improved H-mode scenarios for ITER.

References

[1] G. JANESCHITZ, et al., Plasma Phys. Control. Fusion **44**,No 5A (2002) A459-A471
[2] G.W. PACHER, et al., Nucl. Fusion **43** (2003) 188
[3] G.W. PACHER, H. D. PACHER, G. JANESCHITZ, et al., Proc. 30th EPS Conference on Contr. Fusion and Plasma Phys., St. Petersburg, 2003
[4] G.W. PACHER, H. D. PACHER, G. JANESCHITZ, et al., Plasma Phys. Control. Fusion **46** (2004) A257-A264
[5] H.D. PACHER, et al., J. Nuclear Mater. **313-316C** (2003) 657
[6] A. S. KUKUSHKIN, H. D. PACHER, D. COSTER, et al., Proc. 16th PSI Conference, Portland, 2004, to be published in J. Nucl. Mater.
[7] G. FUSSMANN, et al., Plasma Phys. Contr. Fus. **33** (1991) 1677
[8] A. PANKIN, et al., "Combined Model for the H-mode Pedestal and ELMs", submitted to Plasma Phys. Control. Fusion
[9] A.C.C. SIPS, et al., Plasma Phys. Control. Fusion **44** (2002) B69-B83
[10] I. VOITSEKHOVITCH, et al., Phys. Plasmas **9**, no. 11, (2002) pp. 4671-4684
[11] F. ROMANELLI and F. ZONCA, Phys. Fluids B **5** (11), (1993) p. 481
[12] A.C.C. SIPS, et al., 30th EPS Conference on Contr. Fusion and Plasma Physics, ECA Vol. **27A** (2003), O-1.3A
[13] R. BALET, et al., 25th EPS Conf. on Contr. Fusion and Plasma Physics, ECA Vol. **22C** (1998) 325-328.